

Phonon density of states of Fe₂O₃ across high-pressure structural and electronic transitionsJung-Fu Lin,^{1,*} John S. Tse,² Esen E. Alp,³ Jiyong Zhao,³ Michael Lerche,⁴ Wolfgang Sturhahn,³
Yuming Xiao,⁵ and Paul Chow⁵¹*Department of Geological Sciences, Jackson School of Geosciences, The University of Texas at Austin, Austin, Texas 78712, USA*²*Department of Physics and Engineering Physics, University of Saskatchewan, Saskatoon, SK S7N 5E2, Canada*³*Advanced Photon Source, Argonne National Laboratory, Argonne, Illinois 60439, USA*⁴*McClellan Nuclear Research Center, University of California, Davis, McClellan, California 95652, USA*⁵*HPCAT, Carnegie Institution of Washington, Advanced Photon Source, Argonne National Laboratory, Argonne, Illinois 60439, USA*

(Received 16 May 2011; published 24 August 2011)

High-pressure phonon density of states (PDOS) of Fe₂O₃ across structural and electronic transitions has been investigated by nuclear resonant inelastic x-ray scattering (NRIXS) and first-principles calculations together with synchrotron Mössbauer, x-ray diffraction, and x-ray emission spectroscopies. Drastic changes in elastic, thermodynamic, and vibrational properties of Fe₂O₃ occur across the Rh₂O₃(II)-type structural transition at 40–50 GPa, whereas the Mott insulator-metal transition occurring after the structural transition only causes nominal changes in the properties of the Fe₂O₃. The observed anomalous mode-softening behavior of the elastic constants is associated with the structural transition at 40–50 GPa, leading to substantial changes in the Debye-like part of the PDOS in the terahertz acoustic phonons. Our experimental and theoretical studies provide new insights into the effects of the structural and electronic transitions in the transition-metal oxide (TMO) compounds.

DOI: [10.1103/PhysRevB.84.064424](https://doi.org/10.1103/PhysRevB.84.064424)

PACS number(s): 63.20.dd, 61.50.Ks, 71.20.Be, 72.80.Ga

I. INTRODUCTION

Hematite (Fe₂O₃), an antiferromagnetic insulator under ambient conditions, is regarded as an archetypal Mott insulator for the trivalent transition-metal oxides (TMOs), the majority of which crystallize in the corundum-type structure.^{1,2} Since iron is the most abundant transition metal in the Earth, hematite as an end-member ferric iron (Fe³⁺) oxide is also an important proxy for characterizing the oxidation state, geomagnetism, and geochemistry of the planet's interior.^{3–5} Recent multidisciplinary studies have shown that hematite undergoes a number of transitions under high pressures including structural, insulator-metal, magnetic collapse, and electronic spin-pairing transitions.^{5–18} Of particular interest is the pressure-induced Mott insulator-metal transition with the breakdown of the strong electronic *d-d* correlation and closure of the Mott-Hubbard *d-d* band gap, resulting in a metallic phase with zero moment at approximately 50 GPa.^{1,10–12,18} Although the Mott transition was first proposed to occur concurrently with the Rh₂O₃(II)-type structural and electronic transition, effectively decreasing the Fe³⁺ radius and the unit cell volume in the shift to the low-spin paramagnetic state, the metallic state is reported to occur in the Rh₂O₃(II)-type phase.^{5–18} This observation calls for further understanding on the interplay and associated effects between the structural, electronic, and magnetic transitions in Fe₂O₃ at high pressures.

Electronic and structural transitions in the TMOs have been recently found to significantly affect their physical and chemical properties under high pressures.^{19–25} Specifically, the electronic spin-pairing transition of iron in ferropicroclase ((Mg,Fe)O), an abundant mineral in the Earth's lower mantle, is found to result in changes in density, some of the elastic constants, and transport and rheological properties, which in turn affect a broad spectrum of geophysical, geochemical, and geodynamic implications of the deep Earth.^{22–24} Furthermore, recent studies in the TMOs under high pressures also show anomalous softening in elasticity as a result of the strong

phonon-magnon coupling, leading to substantial changes in the Debye-like part of the phonon density of states (PDOS).^{19,20} Understanding the high-pressure PDOS behavior of hematite is particularly interesting because of the multiple aforementioned transitions and their potential couplings. Yet, the effects of these transitions on elastic, thermodynamic, and vibrational properties of Fe₂O₃ remain largely lacking. Here we have measured the partial PDOS of iron in Fe₂O₃ by nuclear resonant inelastic x-ray scattering (NRIXS) up to 85 GPa in a diamond anvil cell (DAC). NRIXS is a relatively new synchrotron technique that has been successfully applied to study lattice dynamics of ⁵⁷Fe-containing compounds under extreme pressures and temperatures.^{25–28} Together with first-principles theoretical calculations, the PDOS are used to characterize the behavior of Fe₂O₃ across the structural and electronic transitions. We observed significant softening in the elastic properties as well as other major changes in thermodynamic and vibrational properties of Fe₂O₃ between 40 and 50 GPa, which are attributed to the structural transition in hematite. The magnetic collapse is reported to occur in the Rh₂O₃(II) phase between 55 GPa and 75 GPa, causing only nominal changes in the PDOS of the Fe₂O₃.

II. EXPERIMENTAL DETAILS

⁵⁷Fe-enriched Fe₂O₃ (>95% enrichment) was purchased from the Cambridge Isotope Laboratories, Inc., and was characterized for its crystal structure and chemical composition by x-ray diffraction and electron-microprobe analyses, respectively. Samples measuring approximately 25- μ m thick and 40- μ m wide were loaded into DACs with 300- μ m-flat culets or beveled diamonds (150 μ m in the inner culets and 300 μ m in the outer culets) with Be gaskets of 3 mm in diameter and cubic BN-gasket inserts. Pressures were determined from the ruby spheres in the sample chamber using the ruby fluorescence scale.²⁹ High-pressure NRIXS experiments were conducted at sector 3 of the Advanced Photon Source, Argonne

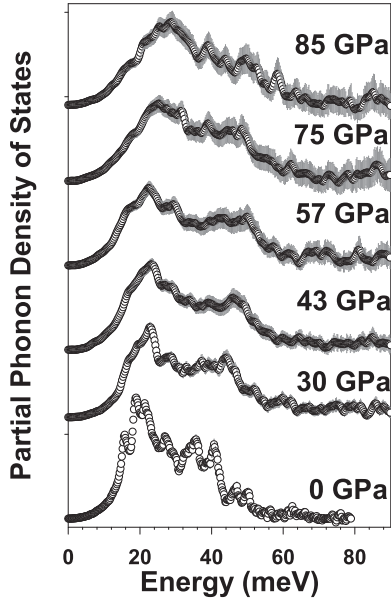


FIG. 1. Representative PDOS of Fe from $^{57}\text{Fe}_2\text{O}_3$ at high pressures. The PDOS spectra are derived from the NRIXS experiments in a high-pressure DAC. Experimental error bars are shown as vertical gray bars.

National Laboratory.^{25–28} Energy spectra were obtained by tuning the x-ray energy (approximately ± 80 to ± 95 meV in steps of 0.25 meV) around the nuclear transition energy of 14.4125 keV with an energy resolution of 1 meV and an x-ray beam size of approximately 10 μm . The $K\alpha, \beta$ -fluorescence radiation from the ^{57}Fe -enriched Fe_2O_3 sample, emitted with time delay relative to the incident x-ray pulses due to the lattice excitations of the iron sublattice, was collected by three avalanche photodiode detectors, whereas the synchrotron Mössbauer spectroscopy (SMS) spectra were collected by a fourth detector in the forward direction. A quasi-harmonic model was used to extract the PDOS from the measured energy spectra (Fig. 1).^{25–27} In this model the atomic motions relative to the temperature-dependent averaged position are assumed to be harmonic under the given conditions of pressure, temperature, and other parameters. Thermal effects such as change of force constants with atomic distances are allowed to change, but the vibrations are still assumed to occur in a harmonic potential.^{25–27} Previous studies have confirmed the reliability of this model to extract the PDOS and the bulk Debye sound velocity (V_D) of Fe-containing compounds under high pressures.²⁸

III. EXPERIMENTAL RESULTS

Elastic, thermodynamic, and vibrational properties of the iron component in Fe_2O_3 have been derived from the integration of the measured PDOS in Fe_2O_3 (Figs. 1 and 2). The V_D of the sample is derived from parabolic fitting of the low-energy slope of the PDOS in the range of approximately 0.2 meV to 15 meV (Fig. 2).^{26,27} In this lattice dynamics model, the Debye velocity of a material is derived from the initial slope of the density of states (DOS) versus energy squared (E^2) plot (a parabolic function in the PDOS versus

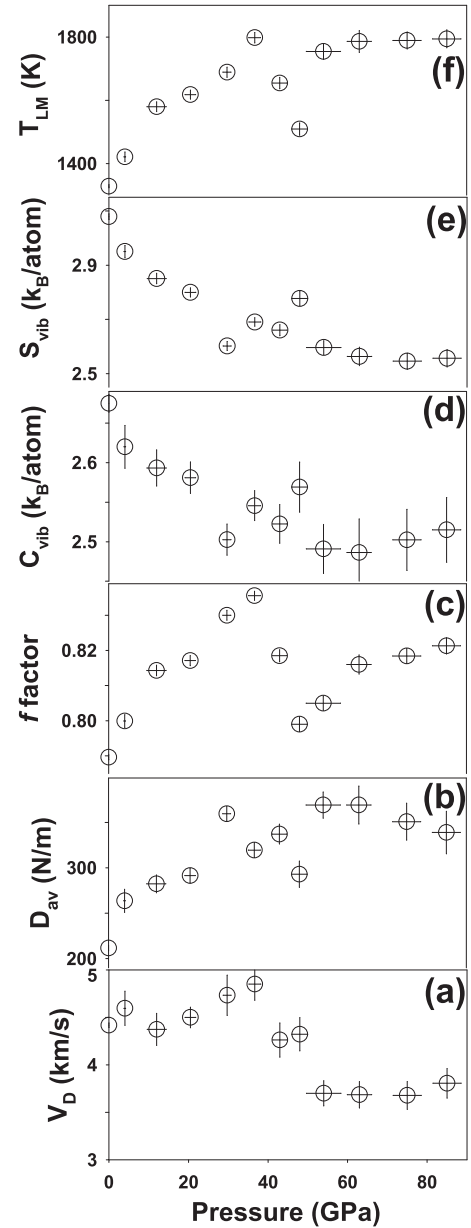


FIG. 2. Elastic, thermodynamic, and vibrational parameters of Fe_2O_3 as a function of pressure obtained from integration of the PDOS. (a) Debye sound velocity; (b) mean force constant, D_{av} ; (c) Lamb-Mössbauer factor, f_{LM} ; (d) vibrational specific heat, C_{vib} (k_B , Boltzmann constant); (e) vibrational entropy, S_{vib} ; (f) characteristic temperature or Lamb-Mössbauer temperature, T_{LM} . We note that these values only represent the contribution of the Fe sublattice in Fe_2O_3 . Using the theoretical densities we computed the sound velocities of Fe_2O_3 in the corundum structure at 40 GPa and $\text{Rh}_2\text{O}_3(\text{II})$ structure at 70 GPa to be 4.7 km/s and 3.8 km/s, respectively.

energy). In the acoustic region, the translation motions of all the atoms in the system (in this case both Fe and O) are in phase. Therefore, the Debye velocity estimated from the Fe PDOS should be exactly the same as that from the full consideration of the DOS. The Debye theory is valid for the acoustic modes in the harmonic solids with Debye-like low-frequency dynamics, and Fe_2O_3 has been shown to exhibit Debye-like lattice-dynamic behavior in previous studies.²⁸

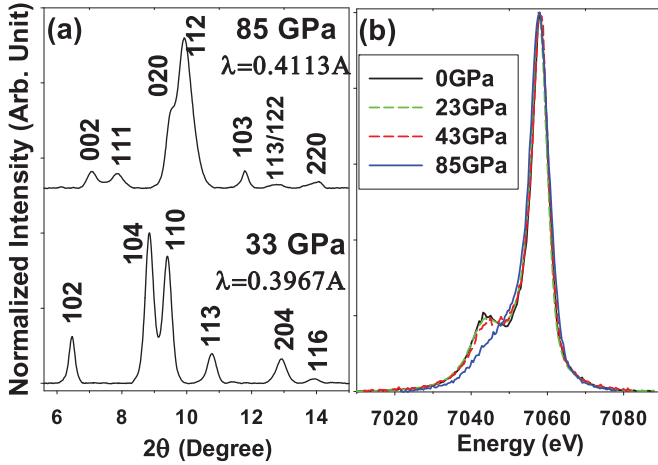


FIG. 3. (Color online) Representative (a) x-ray diffraction and (b) Fe-K β x-ray emission patterns of Fe₂O₃ at high pressures. X-ray diffraction spectra confirmed the structural transition from the corundum-type to the Rh₂O₃(II)-type phase at high pressures. The intensity of the satellite K β ' peak can be used to understand the electronic spin pairing and metallization in Fe₂O₃. Its intensity remains similar across the structural transition but reduces significantly at higher pressures.

It has also been demonstrated that the Debye sound velocity (V_D) measured in NRIXS corresponds to the V_D of the whole matrix (not the Fe atoms alone).²⁸ That is, the projected DOS of Fe represents the total PDOS of Fe₂O₃ in the low-frequency region. For this reason the extraction of the long wavelength properties of the Fe₂O₃ from just the Fe-partial DOS is thus in principle valid.

The characteristic temperature or Lamb-Mössbauer temperature (T_{LM}) in Fig. 2 is defined as

$$\frac{1}{T_{LM}} = k_B \int \frac{2E_{\text{recoil}}}{E^2} g(E) dE,$$

where k_B is the Boltzmann's constant, E_{recoil} is the recoil energy for ⁵⁷Fe nucleus (1.96 meV), and $g(E)$ is the partial PDOS. The recoil-free fraction, commonly known as Lamb-Mössbauer factor (f_{LM}), is related to the characteristic temperature, or Lamb-Mössbauer temperature (T_{LM}), as follows:

$$-\ln f_{LM}(T) = \frac{T}{T_{LM}} = k_0^2 \langle x^2 \rangle,$$

where k_0 is the momentum of the photons with 14.412 keV, which equals to 7.3 Å, and $\langle x^2 \rangle$ is the average displacement. One can also relate T_{LM} to the Debye temperature as

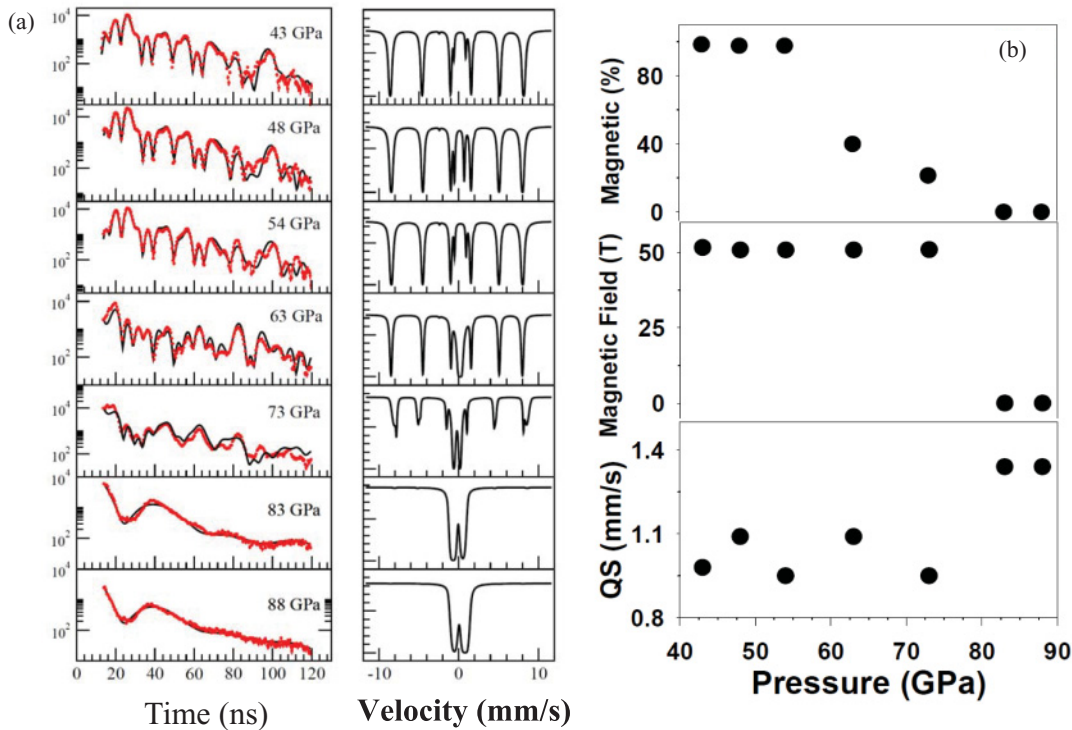


FIG. 4. (Color online) (a) Representative synchrotron Mössbauer spectra of Fe₂O₃ at high pressures. Corresponding energy spectra calculated from the fits are shown in the right panels. Red dots: experimental SMS spectra; black lines: modeled spectra. (b) Analyzed hyperfine parameters and percentage of the magnetic phase in high-pressure Fe₂O₃. Up to 55 GPa the only spectral component is that of the low-pressure magnetic phase characterized by the hyperfine field of 51 T, a typical value of the hyperfine field for ionic ferric-oxide bonding. A NM quadrupole-splitting component emerges at approximately 55 GPa, which we assigned as the high-pressure component, coexisting with the low-pressure magnetic-split component. The relative abundance of the low-pressure component continues to decrease until the magnetic collapse is completed at around 75 GPa. We note that the hyperfine field of the magnetic component is slightly reduced by about 10% within the transition.

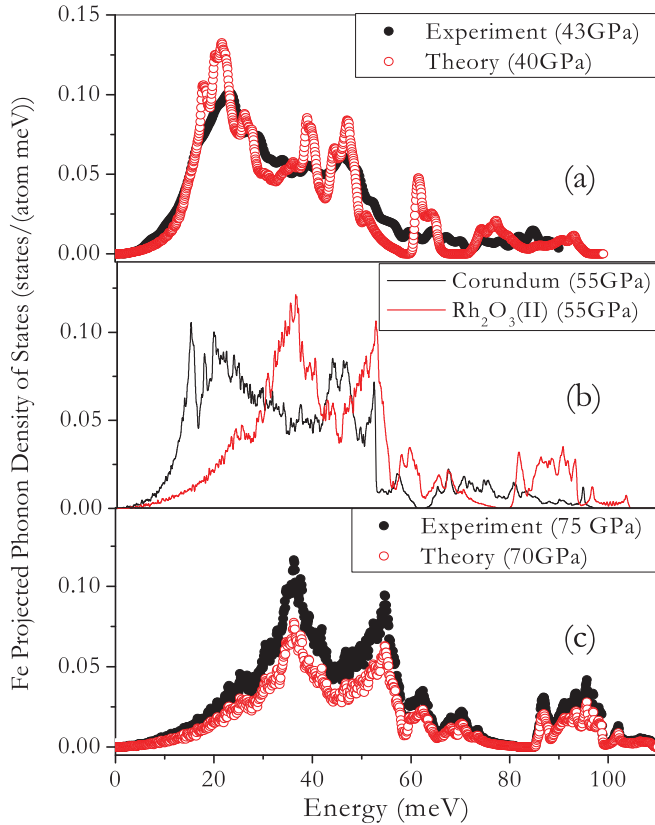


FIG. 5. (Color online) Projected Fe vibrational PDOS of Fe_2O_3 at high pressure from first-principles calculations. (a) The AFM corundum-type phase at 40 GPa. (b) The theoretical AFM corundum-type phase (black line) and the NM $\text{Rh}_2\text{O}_3(\text{II})$ -type phase (red line) at 55 GPa. Black lines: corundum-type phase; red lines: $\text{Rh}_2\text{O}_3(\text{II})$ -type phase. (c) The NM $\text{Rh}_2\text{O}_3(\text{II})$ -type phase at 75 GPa. The black and red circles in (a) and (c) represent the experimental and theoretical Fe PDOS, respectively.

follows:

$$-\ln f_{\text{LM}}(T) = k_B T \frac{6E_{\text{Recoil}}}{E_D^2(T)},$$

where E_D is the Debye cut-off energy, as given by the maximum in the Debye distribution of the PDOS. Hence,

$$T_{\text{LM}} = \frac{E_D^2}{6k_B E_{\text{Recoil}}}.$$

Abnormal behavior of these properties is observed to occur between 40 GPa and 50 GPa. Specifically, V_D , the mean force constant (D_{av}), and the Lamb-Mössbauer factor (f_{LM}) suddenly drop between 40 and 50 GPa, suggesting a softening in Fe_2O_3 in this pressure range. Furthermore, vibrational specific heat (C_{vib}) and vibrational entropy (S_{vib}) decrease with increasing pressures but jump significantly between 40 and 50 GPa. To understand these observations, we have employed x-ray diffraction, SMS, and x-ray emission spectroscopy (XES) to confirm the crystal structures, hyperfine parameters, and total-spin momentum of Fe_2O_3 under high pressures, respectively (Figs. 3 and 4). X-ray diffraction spectra were consistent with a structural transition from the corundum to the $\text{Rh}_2\text{O}_3(\text{II})$ structure that has been reported

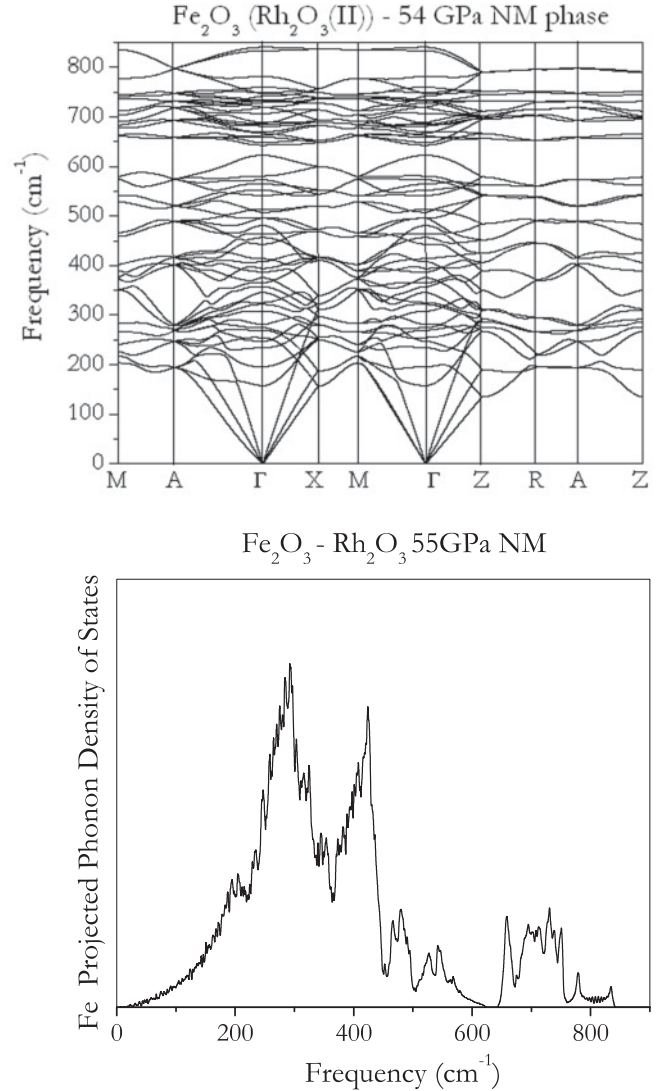


FIG. 6. Calculated phonon dispersive curves (top) and Fe-projected DOS (bottom) of the NM $\text{Rh}_2\text{O}_3(\text{II})$ structure of Fe_2O_3 at 55 GPa using the GGA method.

to occur at approximately 40–50 GPa,^{7–10} whereas the SMS and XES results indicated that the magnetic collapse occurs in the high-pressure $\text{Rh}_2\text{O}_3(\text{II})$ phase and is completed at approximately 75 GPa, consistent with previous studies^{5–15,18} (Figs. 3 and 4).

IV. THEORETICAL CALCULATIONS

In order to qualitatively decipher the interplay between the structural, magnetic, and electronic transitions of Fe_2O_3 under high pressures, first-principles electronic and phonon calculations using the VASP suite program were performed to investigate structural and magnetic transitions in hematite (Figs. 5–8).^{30–33} Projected augmented potentials were used for both the Fe and O atoms, and the semi-core 3s and 3p orbitals of Fe were treated as valence.^{31,32} The rotationally invariant LSDA + U model with the Perdew-Burke-Ernzerhof exchange-correlation function ($U = 4.0$ eV and $J = 0.9$ eV) in the generalized gradient approximation (GGA) was used to model the strongly correlated Fe 3d states in the

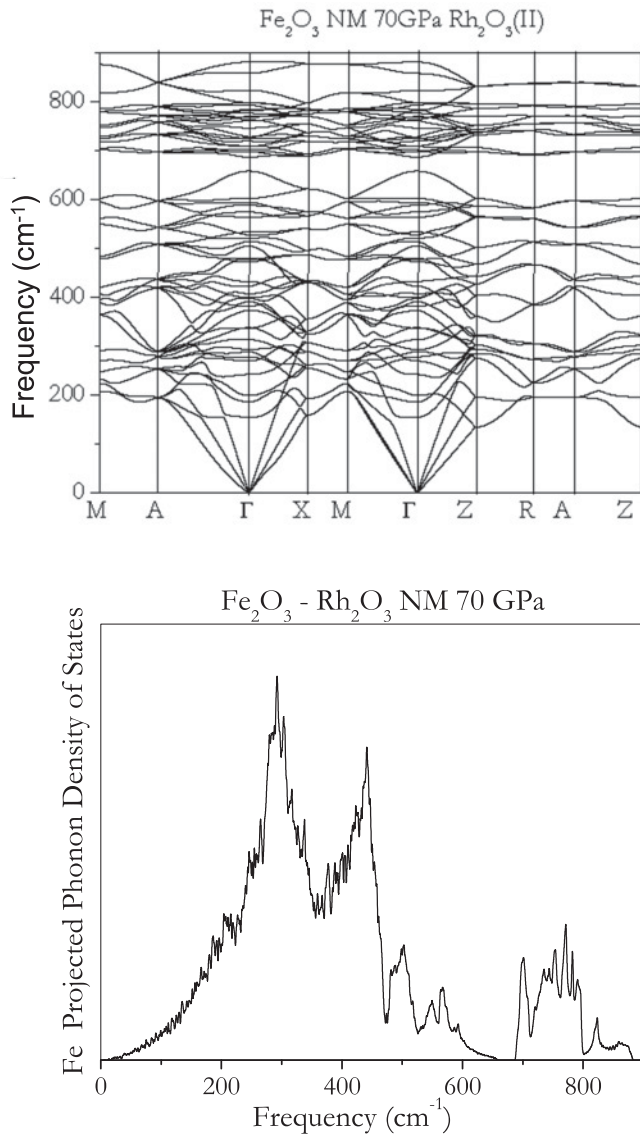


FIG. 7. Calculated phonon dispersive curves (top) and Fe-projected DOS (bottom) of the NM Rh_2O_3 (II) structure of Fe_2O_3 at 70 GPa using the GGA method.

antiferromagnetic (AFM) corundum structure.^{30–32} Based on previous studies,¹⁴ we have used the Rh_2O_3 (II)-type structure (space group: $Pbcn$) with experimentally reported lattice parameters for our theoretical calculations for the high-pressure phase.¹⁴ It is well known that it is necessary to include the Hubbard U to describe the band gap of the insulating magnetic state. Whether it is necessary to involve the Hubbard U term to describe the metallic nonmagnetic state is not certain. We have performed calculations with the same Hubbard U parameter as in the corundum structure, but the calculated PDOS does not agree with the experimental results at all. The GGA method, on the other hand, agrees well with experiments, leading us to rule out the use of the Hubbard U in the calculations. It is found that the GGA approximation is consistent with experimental results and adequate to describe the electron and phonon structures of the high pressure nonmagnetic (NM) Rh_2O_3 (II) phase (Fig. 5).³⁴ Phonon dispersion and Fe-projected DOS were calculated with the small displacement method³³ employing

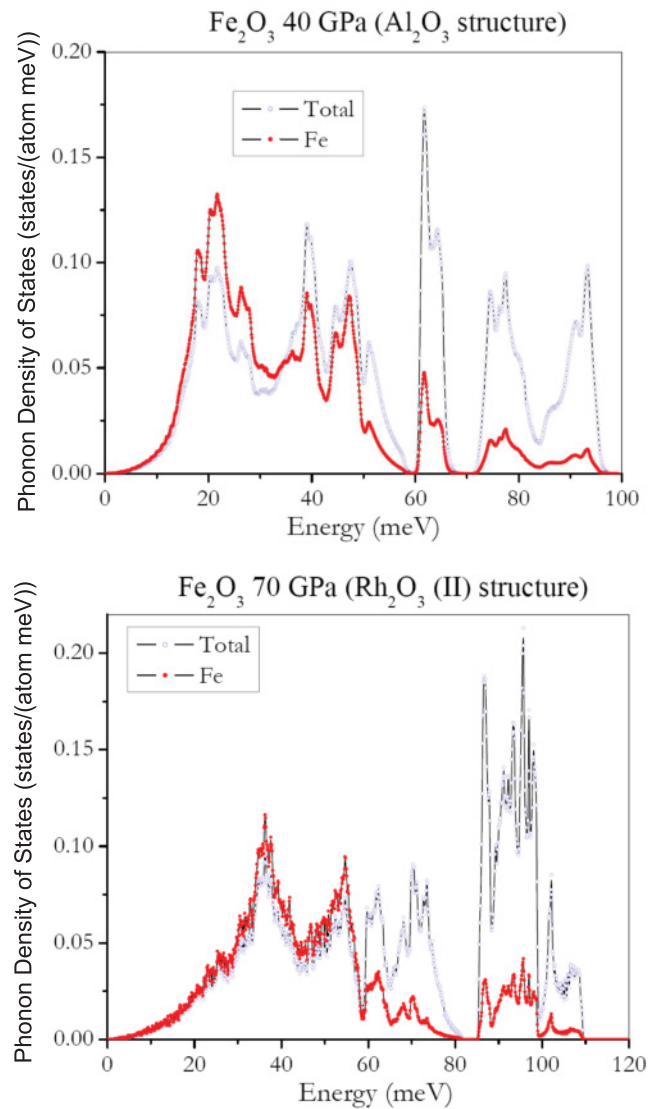


FIG. 8. (Color online) Calculated Fe-projected DOS and total DOS of Fe_2O_3 in the corundum structure (top) and Rh_2O_3 (II) structure (bottom).

supercells constructed from a $2 \times 2 \times 2$ replicate of the corundum structure and a $1 \times 2 \times 2$ replicate of the Rh_2O_3 (II) crystallographic unit cell. Calculations were performed at 40 GPa for the AFM corundum-type phase, at 55 GPa for both the NM corundum-type phase and AFM Rh_2O_3 (II)-type phase, and at 70 GPa for the NM Rh_2O_3 (II) (Figs. 5–8). We have also calculated the stability of the NM corundum and AFM Rh_2O_3 (II) structures at these pressures and have found them to be unstable when compared to the AFM corundum and NM Rh_2O_3 (II) structures.

The theoretical Fe PDOS of the AFM corundum structure at 40 GPa and the NM Rh_2O_3 (II) structure at 70 GPa are compared with corresponding experimental results in Fig. 5(a) and 5(c), respectively. The experimentally observed decrease in V_D of 14% from the magnetic corundum to metallic Rh_2O_3 (II) phase is correctly reproduced by the calculated value of 16% (Figs. 2 and 5). The agreements are very good, and all the salient features of the experimental PDOS are

correctly reproduced. The most distinctive differences in the calculated vibrational PDOS features are the drastic shift of the first PDOS peak from approximately 21 meV in the AFM corundum-type phase to approximately 37 meV in the AFM Rh₂O₃(II)-type structure at 55 GPa, and as a consequence, a significant drop in the gradient of the acoustic phonon dispersion. These predictions are qualitatively consistent with experimental observations on the softening of the Debye sound velocity across the structural transition (Figs. 1 and 5). There are also shifts in the high-frequency vibrations, dominated by the oxygen motions, to higher energy. Across the structural transition, the Debye sound velocity suddenly becomes much slower in the Rh₂O₃(II)-type phase than in the corundum-type phase; though, it should be noted that these phases are all in the AFM state. In absence of the structural transition, the low-frequency Debye-like vibrations in the corundum-type and the Rh₂O₃(II)-type structures, respectively, behave rather normally with a weak pressure effect; this weak pressure effect persists across the AFM to the NM transition in the Rh₂O₃(II)-type phase, suggesting that electronic transitions do not significantly affect elastic and vibrational properties of Fe₂O₃ at high pressures.

V. DISCUSSION

Based on our experimental results and first-principles calculations, here we address how the properties of Fe₂O₃ are affected by structural and electronic transitions under high pressures. Together with the previous studies, it is now well documented that the transition from the AFM hematite to the AFM Rh₂O₃(II) phase occurs at approximately 40–50 GPa with a volume reduction of approximately 10% and shortening of the bond lengths.^{5–15} Our observed dramatic changes in the elastic, vibrational, and thermodynamic properties correspond to the structural transition to the AFM Rh₂O₃(II)-type occurring at 40–50 GPa, without the involvement of the spin-pairing and magnetic-collapse transitions. This structural transition is thus associated with the softening in the lattice vibrational phonons in Fe₂O₃ and significant reductions in the V_D , Lamb-Mössbauer factor, and the mean-force constant, among others. The drop in the V_D across the transition suggests that compressional and shear velocities of Fe₂O₃ would also decrease significantly as well. On the other hand the mean-force constant represents the short-range repulsive, interatomic forces arising from the charge distributions and Hund's rules of atoms, and its decrease thus corresponds to a softening in the lattice incompressibility and likely the lattice strength within the transition. The Lamb-Mössbauer factor is related to the mean-square displacement of the iron atoms in the lattice, $\langle x^2 \rangle$, through $f_{LM} = \exp(-k^2 \langle x^2 \rangle)$, where k is the wave number of the resonant x-ray. That is, the structural transition reduces the lattice displacement of the Fe³⁺ atoms

and is manifested in the reduction of the Lamb-Mössbauer factor by approximately 5%. This transition also results in an increase in the thermodynamic vibrational heat capacity and entropy.

Previous studies showed that the electronic transition and the magnetic collapse, the Mott transition, occur at higher pressures only in the Rh₂O₃(II) phase.¹³ A Mott transition, as defined by Mott himself, is an isostructural paramagnetic metal to paramagnetic insulator transition.^{1,21} This isostructural transition implies that the crystal symmetry of the Rh₂O₃(II) phase is preserved across the magnetic collapse. Our studies, together with previous results,^{7–14} confirm this behavior, in which the AFM character with magnetic moments persists up to approximately 75 GPa before the magnetic collapse is fully completed. Based on our NRIXS results and first-principles calculations, the Mott transition does not significantly affect the elastic, thermodynamic, and vibrational properties of the Rh₂O₃(II)-type Fe₂O₃; these properties change rather monotonically with increasing pressures (Fig. 2). The high-spin AFM Rh₂O₃(II)-type phase is found to be dynamically unstable at 55 GPa in our calculations, and a soft phonon mode is found at the M-symmetry point.

VI. CONCLUSIONS

In summary significant changes in the PDOS of Fe₂O₃ were observed with the softening on the sound velocities, interatomic-force constant, and Lamb-Mössbauer factor associated with the corundum-type to the Rh₂O₃(II)-type structural transition at 40–50 GPa, but the isostructural Mott transition only occurs in the Rh₂O₃(II) phase and does not have a strong effect on the properties of Fe₂O₃. The structural transition under pressure corresponds to anomalous mode-softening behavior of the elastic constants preceding the Mott transition, leading to substantial changes in the Debye-like part of the PDOS in the terahertz acoustic phonons. Our studies on the high-pressure behavior of the archetypal Fe₂O₃ provide new insights into the effects of the structural and electronic transitions in the TMO compounds.

ACKNOWLEDGMENTS

We acknowledge XOR-3 and GSECARS, APS, and ANL for the use of the synchrotron and laser facilities and TACC for the computational facilities. Use of the Advanced Photon Source was supported by US Department of Energy (DOE), Office of Science, Basic Energy Sciences (BES), under contract No. DE-AC02-06CH11357. J.F.L. acknowledges financial support from Energy Frontier Research in Extreme Environments (EFREE) Center, NSF Earth Sciences (EAR-0838221), and Carnegie/DOE Alliance Center (CDAC). M.L. acknowledges financial support from COMPRES.

*Corresponding author: afu@jsg.utexas.edu

¹N. Mott, *Metal-Insulator Transitions* (Taylor & Francis, London, 1974), pp. 294.

²I. S. Lyubutin, S. G. Ovchinnikov, A. G. Gavriluk, and V. V. Struzhkin, *Phys. Rev. B* **79**, 085125 (2009).

³D. P. Dobson and J. P. Brodholt, *Nature* **434**, 371 (2005).

⁴C. McCammon, *Science* **308**, 807 (2005).

⁵E. Ito, H. Fukui, T. Katsura, D. Yamazaki, T. Yoshino, Y. Aizawa, A. Kubo, S. Yokoshi, K. Kawabe, S. Zhai, A. Shatzkiy, M. Okube, A. Nozawa, and K.-I. Funakoshi, *Am. Mineral.* **94**, 205 (2009).

- ⁶R. D. Shannon and C. T. Prewitt, *J. Solid State Chem.* **2**, 134 (1970).
- ⁷T. Yagi and S. Akimoto, in *High Pressure Research in Geophysics*, edited by S. Akimoto and M. Manghnani (Kluwer Academic, Tokyo, 1982), p. 81.
- ⁸Y. Syono, A. Ito, S. Morimoto, S. Suzuki, T. Yagi, and S. Akimoto, *Solid State Commun.* **50**, 97 (1984).
- ⁹E. Knittle and R. Jeanloz, *Solid State Commun.* **58**, 129 (1986).
- ¹⁰J. S. Olsen, C. Cousins, L. Gerward, H. Jhans, and B. Sheldon, *Phys. Scr.* **43**, 327 (1991).
- ¹¹M. P. Pasternak, G. Kh. Rozenberg, G. Yu. Machavariani, O. Naaman, R. D. Taylor, and R. Jeanloz, *Phys. Rev. Lett.* **82**, 4663 (1999).
- ¹²J.-P. Rueff, C.-C. Kao, V. V. Struzhkin, J. Badro, J. Shu, R. J. Hemley, and H.-K. Mao, *Phys. Rev. Lett.* **82**, 3284 (1999).
- ¹³J. Badro, G. Fiquet, V. V. Struzhkin, M. S. Somayazulu, H. K. Mao, G. Shen, and T. Le Bihan, *Phys. Rev. Lett.* **89**, 205504 (2002).
- ¹⁴G. K. Rozenberg, L. S. Dubrovinsky, M. P. Pasternak, O. Naaman, T. LeBihan, and R. Ahuja, *Phys. Rev. B* **65**, 064112 (2002).
- ¹⁵S. Ono, T. Kikegawa, and Y. Ohishi, *J. Phys. Chem. Solids* **65**, 1527 (2004).
- ¹⁶J. Kunes, D. M. Korotin, M. A. Korotin, V. I. Anisimov, and P. Werner, *Phys. Rev. Lett.* **102**, 146402 (2009).
- ¹⁷N. C. Wilson and S. P. Russo, *Phys. Rev. B* **79**, 094113 (2009).
- ¹⁸S. Wang, W. L. Mao, A. P. Sorini, C.-C. Chen, T. P. Devereaux, Y. Ding, Y. Xiao, P. Chow, N. Hiraoka, H. Ishii, Y. Q. Cai, and C.-C. Kao, *Phys. Rev. B* **82**, 144428 (2010).
- ¹⁹V. V. Struzhkin, H. K. Mao, J. Hu, M. Schwoerer-Böhning, J. Shu, R. J. Hemley, W. Sturhahn, M. Y. Hu, E. E. Alp, P. Eng, and G. Shen, *Phys. Rev. Lett.* **87**, 255501 (2001).
- ²⁰A. P. Kantor, S. D. Jacobsen, I. Yu. Kantor, L. S. Dubrovinsky, C. A. McCammon, H. J. Reichmann, and I. N. Goncharenko, *Phys. Rev. Lett.* **93**, 215502 (2004).
- ²¹C. S. Yoo, B. Maddox, J.-H. P. Klepeis, V. Iota, W. Evans, A. McMahan, M. Y. Hu, P. Chow, M. Somayazulu, D. Hausermann, R. T. Scalettar, and W. E. Pickett, *Phys. Rev. Lett.* **94**, 115502 (2005).
- ²²J. F. Lin, S. D. Jacobsen, W. Sturhahn, J. M. Jackson, J. Zhao, and C. S. Yoo, *Geophys. Res. Lett.* **33**, L22304 (2006).
- ²³D. Antonangeli, J. Siebert, C. M. Aracne, D. L. Farber, A. Bosak, M. Hoesch, M. Krisch, F. J. Ryerson, G. Fiquet, and J. Badro, *Science* **331**, 64 (2011).
- ²⁴R. M. Wentzcovitch, J. F. Justo, Z. Wu, C. R. S. da Silva, D. Yuen, and D. Kohlstedt, *Proc. Natl. Acad. Sci. USA* **106**, 8447 (2009).
- ²⁵W. Sturhahn and K. G. Kohn, *Hyperfine Interact.* **123/124**, 367 (1999).
- ²⁶W. Sturhahn, *Hyperfine Interact.* **125**, 149 (2000).
- ²⁷W. Sturhahn, *J. Phys. Condens. Matter* **16**, S497 (2004).
- ²⁸M. Y. Hu, W. Sturhahn, T. S. Toellner, P. D. Mannheim, D. E. Brown, J. Zhao, and E. E. Alp, *Phys. Rev. B* **67**, 094304 (2003).
- ²⁹H. K. Mao, P. M. Bell, J. W. Shaner, and D. J. Steinberg, *J. Appl. Phys.* **49**, 3276 (1978).
- ³⁰J. P. Perdew, K. Burke, and M. Ernzerhof, *Phys. Rev. Lett.* **77**, 3865 (1996).
- ³¹G. Kresse and J. Furthmuller, *Comp. Mater. Sci.* **6**, 15 (1996).
- ³²G. Kresse and J. Furthmuller, *Phys. Rev. B* **54**, 11169 (1996).
- ³³Z. Li and T. S. Tse, *Phys. Rev. B* **61**, 14531 (2000).
- ³⁴H. W. Sheng, H. W. Sheng, H. Z. Liu, Y. Q. Cheng, J. Wen, P. L. Lee, W. K. Luo, S. D. Shastri, and E. Ma, *Nat. Mater.* **6**, 192 (2007).